Preprints of the 21st IFAC World Congress (Virtual)
Berlin, Germany, July 12-17, 2020

System Identification and Control Design for a Tip Tilt Nanopositioning System

Yu Hsiang Su, David Felipe Morales Aldana and William P. Heath *

** Department of Electrical and Electronic Engineering*
Sackville Street Building
The University of Manchester
Manchester, M13 9PL, UK
yu-hsiang.su@postgrad.manchester.ac.uk
david.moralesaldana@manchester.ac.uk
William.Heath@manchester.ac.uk

Abstract: This paper examines the system identification and control design for a tip tilt nanopositioning stage with an experimental case study based on the Queensgate $NPS-\theta\gamma-2M$ prototype nanopositioning stage that has two degrees of freedom (DOF) of tip tilting motion. The paper presents the multi-input multi-output (MIMO) position model and proposes a MIMO H-infinity control with loop shaping design. The control performance is compared with a benchmark SISO integral control. The H-infinity control has the advantage of increasing the response speed and improving the bandwidth while considering the whole multivariable model in the design scheme and maintaining the control robustness. The experiment results confirm that the MIMO H-infinity control has a better control performance in terms of the response time and bandwidth, compared with the benchmark SISO integral control.

Keywords: Nanopositioning, Tip Tilt, H_∞ Control, Robust Control, Multivariable Control

1. INTRODUCTION

1.1 Research Background

Nanotechnology can be defined as the understanding and control of matter at the nanoscale, in which there is at least one dimension less than 100 nm, and where the unique phenomena at the nanoscale enable novel technology applications (Devasia et al., 2007). Nanopositioners are ultra-precise positioning stages which can be used for high-resolution positioning to achieve the manipulation and control of samples at the nanoscale (Fleming and Leang, 2014), (Eielsen et al., 2014). Moreover, nanopositioning stages are widely used in many nanoscience and nanotechnology applications. These include experimental microscopy, which gives scientists the ability to see and move the samples at the nanoscale, using equipment such as a scanning probe microscope (SPM) and atomic force microscope (AFM) (Gu et al., 2016). In general, nanopositioning stages are driven by piezoelectric actuators which provide large force and precise motion. The systems are also equipped with capacitive sensors which measure position output. However, the inherent creep and hysteresis nonlinearities of piezoelectric actuators and the lightly damped resonant dynamics in the low frequency modes are the main challenging issues which limit the system closed-loop bandwidth (Gu et al., 2016), (Kara-Mohamed et al., 2015). Therefore, research has recently been focusing on the improvements in modelling and control design, to fulfil the demand for high-precision positioning control at high bandwidth for nanopositioning applications (Yong et al., 2008).

Furthermore, nanopositioning stages can be categorised into different types based on their motion, such as translation, rotation, and tip tilting (Fleming and Leang, 2014). For the translational nanopositioning stages, several models and control methods have been proposed in the literature to achieve the different control specifications of applications, and to deal with the system nonlinear effects (Gu et al., 2016). However, the tip tilt nanopositioning stage is a new research area, and the case study of this paper, the Queensgate $NPS-\theta\gamma-2M$ nanopositioning stage, is a prototype. Therefore, the motivation of this research is to study the tip tilt nanopositioning stage, and carry out a procedure to build a suitable position model which represents the system dynamics; and thus to design and compare the performance of two different controllers, such as the classical SISO integral control and the MIMO robust H infinity control with loop shaping design.

In Section 2, modelling and system identification of the tip tilt nanopositioning stage is presented. Section 3 introduces two different control designs for the tip tilt nanopositioning stage. The results of a case study are produced in Section 4 and the conclusion of the paper is presented in Section 5.

1.2 Tip Tilt Nanopositioning Stage

The $NPS-\theta\gamma-2M$ tip tilt nanopositioning stage shown in Fig. 1 is a prototype from Queensgate which has been developed for optical inspection and imaging systems requiring the ultra-high precision positioning of mirrors, such as the precision beam steering and the image jitter correction. The nanopositioning stage provides two degrees of freedom of tip tilting motion on the x and y axes in milliradians with sub-

micro-radian resolutions. In Fig. 1, the black arrows represent the motion axes, and the red arrows represent the tip tilting motion on each axis. The system is driven by the piezoelectric actuators from two input channels and also equipped with capacitive sensors which measure both the position and force output at each axis. To be more specific, the input channels receive the voltage reference signal, while the position sensors measure the tip tilting motion of the nanopositioning stages, and the force sensors measure the force applied from the piezoelectric actuators to the moving stages. Accordingly, the $NPS-\theta\gamma-2M$ nanopositioning stage is a multivariable system which has two input channels and four output channels, including the position and force measurement. Nevertheless, only the measured position outputs are studied in this paper. Therefore, the system can be identified as a two input and two output model.

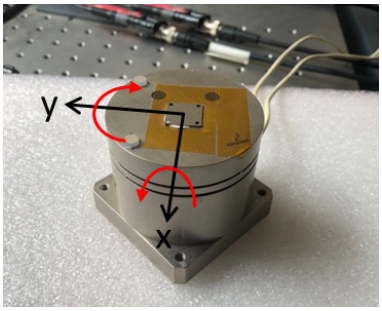

Fig. 1. $NPS-\theta\gamma-2M$ Nanopositioning Stage.

1.3 Schematic Diagram of the Control Structure

Fig. 2 shows the schematic diagram of the experimental control structure for the $NPS-\theta\gamma-2M$ tip tilt nanopositioning stage used in this study. There are two input channels for x and y tip tilting motion and two output channels for the position measurement. First, the LabVIEW control program computes the control input from the given reference and the measurement feedback signals. Then, the Queensgate $NPC-D-5200DS$ digital controller converts the control input to the actual control signal for the nanopositioning stage. Finally, the piezoelectric actuator receives the control input signal and drives the $NPS-\theta\gamma-2M$ tip tilt nanopositioning stage. Specifically, the $NPC-D-5200DS$ digital controller is used to communicate to a PC while LabVIEW is used to control the nanopositioning stage. However, this experimental set up increases some extra loop delay in the control system.

2. MODELLING AND SYSTEM IDENTIFICATION

2.1 Data-driven System Identification

The foundation of all model-based control design is to establish a model which provides information about the system response under input signals and typical disturbances, in order to approximate the actual system (Glad and Ljung, 2000). Furthermore, system identification is the technique of building a model by treating the system as a black box and identifying the input-output dynamics of the system from the excited perturbation input signal and the corresponding output signal (Godfrey et al., 2005). However, the use of piezoelectric actuators introduces nonlinear effects to the nanopositioning stage, such as creep and hysteresis; these increase the difficulty of modelling and system identification in nanopositioning

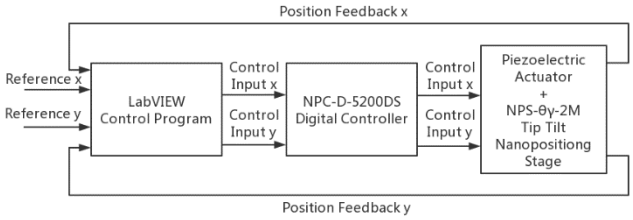

Fig. 2. The Schematic Control Structure of the $NPS-\theta\gamma-2M$ Tip Tilt Nanopositioning Stage.

stages (Devasia et al., 2007). On the other hand, a linear time-invariant (LTI) model is commonly used to approximate the actual nonlinear system, due to its modelling simplicity, the capability to capture most of the system dynamics, and the variety of corresponding control design options (Vaqueiro-Contreras, 2015). In particular, the linear modelling approach using the data-driven system identification techniques is considered in some literature and shows a sufficient modelling accuracy for the feedback control of the nanopositioning stages (Gu et al., 2016), (Kara-Mohamed and Heath, 2016), (Sebastian and Salapaka, 2005), (Das et al., 2015). Nevertheless, it is highly recommended to identify the level of system nonlinear distortion by conducting a nonlinearity identification test before considering a linear model to represent the practical nonlinear system (Vaqueiro-Contreras, 2015), (Kara-Mohamed et al., 2015).

2.2 Model Assumptions and Modelling Procedure

A linear MIMO position model can be identified for the nanopositioning stage with a transfer function matrix as follows

$$\begin{bmatrix} X \\ Y \end{bmatrix} = \begin{bmatrix} G_{11} & G_{12} \\ G_{21} & G_{22} \end{bmatrix} \begin{bmatrix} U_x \\ U_y \end{bmatrix} = G \begin{bmatrix} U_x \\ U_y \end{bmatrix} \quad (1)$$

where X and Y are the output channels which are the position measurement, and U_x and U_y are the voltage inputs to each channel. It is noted that each element of the MIMO transfer function matrix G is assumed to be a linear model.

Furthermore, the exciting signal used for system identification is designed as an inverse-repeat PRBS signal with the even harmonic suppressed, which is proposed to be suitable for linear system identification in the presence of nonlinear distortion (Godfrey et al., 2005). A similar approach to identify the dynamics of nanopositioning system is used by Kara-Mohamed et al. (2015). First, a ninth order PRBS signal with period of 512 elements and a seventh order PRBS signal with period of 254 elements are used to obtain the open loop frequency response of the system. Next, a ninth order PRBS signal is excited at each channel independently, and the outputs of position from both channels are measured to obtain each element of G in (1). Specifically, the outputs X and Y will be respectively related to models G_{11} and G_{21} by exciting the PRBS signal at U_x and setting U_y to zero. Conversely, models G_{12} and G_{22} will be separately related to the output channels X and Y when U_y is excited by the PRBS signal and U_x is set to zero. Further, the best fitting model in the system identification for each element of the MIMO transfer function matrix G is identified by selecting the output error (OE) model

with different orders of polynomial and time delay. The OE model structure is given by

$$y(t) = \frac{B(q)}{F(q)}u(t - nk) + e(t) \quad (2)$$

where $y(t)$ is the output, $u(t)$ is the input, $e(t)$ is the error, q is the difference operator and nk is the order of the delay (Ljung, 1999).

2.3 MIMO Position Model

First, Fig. 3 shows the open-loop frequency response of the diagonal position model G_{11} and the cross-coupling position model G_{12}. Two non-parametric models are obtained and compared by exciting two PRBS signals with the order of ninth and seventh in the open-loop system for each position model. To be more specific, the blue line represents the response of the PRBS signal with the ninth order, while the red line represents the response of the PRBS signal with the seventh order. It can be observed that there is a slight model mismatching between the two non-parametric models in the operating range around the first resonant frequency of the diagonal position model G_{11}. On the other hand, the model discrepancy in the cross-coupling position model G_{12} is more severe around the first resonant frequency. The model mismatching may be affected by the system nonlinearity from the piezoelectric actuator, and by the system uncertainty. It shows that the nonlinear effect has more impact on the cross-coupling position model than the diagonal position model. Moreover, it is noted that the steady state gain of the cross-coupling model is lower compared to the diagonal model. The modelling result of position model G_{22} and G_{21} are not included here as they are similar to the position model G_{11} and G_{12}.

In addition, Fig. 4 displays the absolute value of the Fourier Transform of the position model G_{11} and G_{12}, which reveals the level of the nonlinear distortion in the system response. The output spectrum is plotted by Godfrey's method, which can be used to analyse the nonlinear distortion in the system response (Godfrey et al., 2005), (Schoukens et al., 2003), (Kara-Mohamed et al., 2015). Specifically, the crosses represent the linear response at excited frequencies, while the circles indicate the nonlinear response at the other suppressed frequencies. It can be observed that the linear response has a relatively higher value than the nonlinear response in the whole frequency range for the diagonal model G_{11}. The value of linear response and nonlinear response near the first resonant frequency are closer in the cross-coupling model G_{12} which corresponds to the former result. Nevertheless, it is reasonable to approximate the actual nonlinear nanopositioning system using the linear position model, as the linear response dominates most of the frequency response in the operating frequency region.

Next, Table 1 presents the information of the best-fit position OE models obtained by the MATLAB System Identification Toolbox. It shows that the obtained OE position models have around a 90% fit to the procured data. Moreover, the frequency response of each OE model and the non-parametric model of the MIMO position linear transfer function matrix G are presented in Appendix A and each coefficient of the discrete transfer function of the MIMO position model are presented in Appendix B.

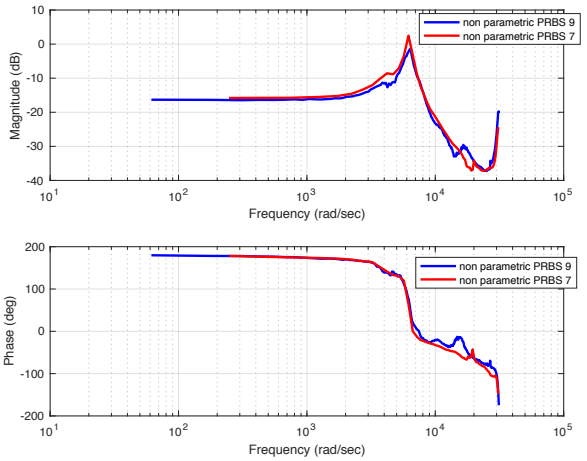

(a) Diagonal position model G_{11}

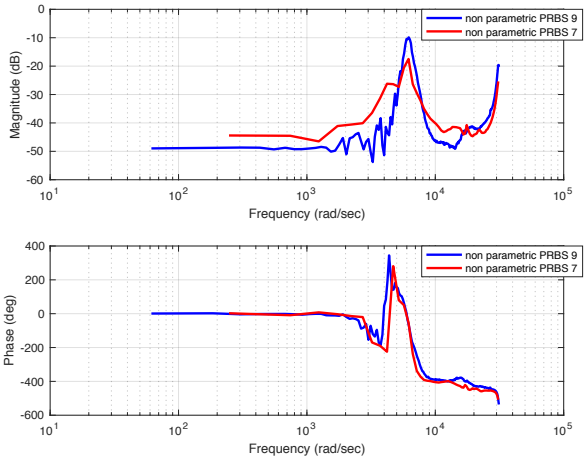

(b) Cross-coupling position model G_{12}

Fig. 3. Frequency Response of Position Model.

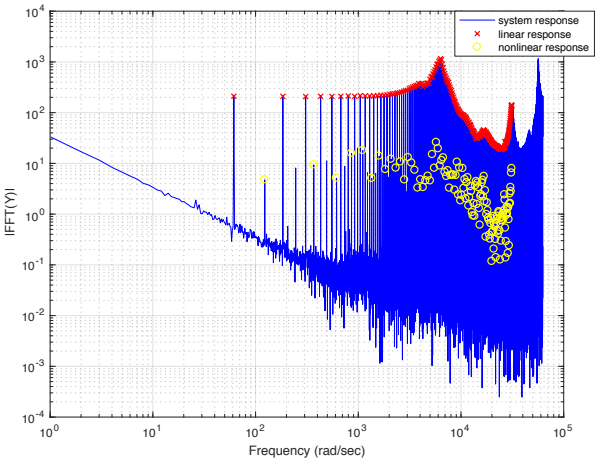

(a) Diagonal position model G_{11}

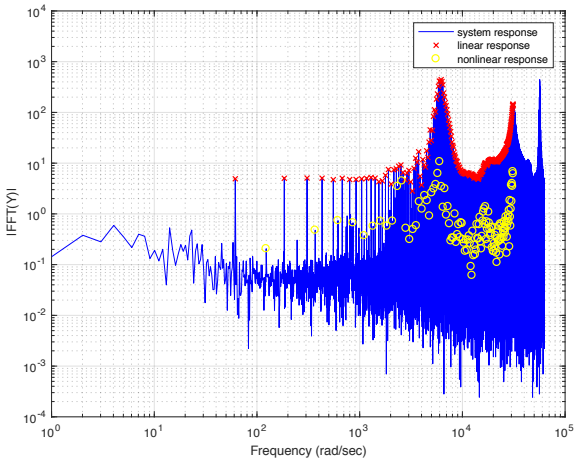

(b) Cross-coupling position model G_{12}

Fig. 4. Position Output Spectrum.

Element	Parameters	Best fit percentage	Validation MSE
G_{11}	$[2, 4, 1]$	89.91	8.837×10^{-5}
G_{12}	$[8, 8, 1]$	91.79	1.217×10^{-5}
G_{21}	$[8, 8, 1]$	90.56	6.628×10^{-6}
G_{22}	$[2, 4, 1]$	92.26	8528×10^{-5}

Table 1. Summary of MIMO Position Model System Identification.

3. CONTROL DESIGN

3.1 Benchmark SISO Integral Control

We implement the integral only control as it is a standard benchmark for commercial nanopositioning stages. The closed-loop bandwidth with integral control is limited to circa 2% of the first resonant frequency (Fleming and Leang, 2014). Commercial nanopositioners achieve higher bandwidth via techniques such as notch filtering, feedforward or the use of force feedback (Fleming and Leang, 2014).

The integral controller is designed in the SISO structure and implemented in the feedback loop as the diagonal control structure, also known as the decentralised control structure is the most straightforward approach among all the multivariable control design (Skogestad and Postlethwaite, 2005). In addition, the error signal is used as the input of the controller, to improve the system tracking performance and compensate for the modelling uncertainty. Therefore, the feedback SISO integral controller has the robustness to modelling error, and the ability to reduce the nonlinear effect of the piezoelectric actuator at low frequencies (Fleming and Leang, 2014). The aim of designing a classical SISO integral controller is to set up a standard control performance that can be compared with the other control designs.

The diagonal SISO integral control structure can be represented as

$$C = \begin{bmatrix} C_{Ix} & 0 \\ 0 & C_{Iy} \end{bmatrix} \tag{3}$$

Each element of the controller C in (3) is designed in discrete form, and the transfer function is given by

$$C_I(z) = K_i \cdot T_s \frac{1}{z-1} \tag{4}$$

where K_i is the integral gain and T_s is the sampling time.

For the $NPS - \theta\gamma - 2M$ tip tilt nanopositioning stage, two discrete SISO integral controllers are designed based on the diagonal position models G_{11} and G_{22} separately, as the system has two DOF and the diagonal position models are not identical. It is noted that the cross-coupling position models G_{12} and G_{21} are neglected in order to simplify the design procedure, as their gains at low bandwidth are relatively smaller than those of the diagonal models, according to the modelling results in Section 2.3.

The integral gains are designed following the closed-loop stability condition from Fleming's recommendation that the maximum integral gain is equal to twice the multiplication of the natural frequency and the damping ratio, which is given by

$$K_i = 2\omega_n\zeta \tag{5}$$

where ω_n is the natural frequency, and ζ is the damping ratio of the diagonal models (Fleming and Leang, 2014).

Table 2 presents the designed integral gains, the natural frequency and damping ratio of the diagonal position models.

Element	G_{11}	G_{22}
Natural Frequency (rad/sec)	6307	5883
Damping ratio	0.082	0.0635
Integral gain K_i	1034.348	747.141

Table 2. Natural Frequency, Damping Ratio and Integral Gain of the Diagonal Position Models.

3.2 MIMO Robust H-infinity Control with Loop Shaping Design

The robust H-infinity control with loop shaping design, using the Glover-McFarlane method, is applied to design a MIMO robust controller for the $NPS - \theta\gamma - 2M$ tip tilt nanopositioning stage (McFarlane and Glover, 1992). The aims of designing the MIMO robust H-infinity control are to improve the system closed-loop bandwidth and the response time. It is noted that the MIMO robust H-infinity control can reduce the system cross-coupling effect as it considers the whole multivariable position model.

The design of the robust H-infinity control starts by defining the nominal plant and its coprime factorisation (Bongers and Bosgra, 1993). First, the left fractional representation of the nominal plant is given by

$$G = \widetilde{M}^{-1}\widetilde{N} \tag{6}$$

where G is the MIMO position transfer function and $\widetilde{M}$ and $\widetilde{N}$ are stable transfer functions. Then, the left coprime factor perturbed system G_Δ can be represented by

$$G_\Delta = \left(\widetilde{M} + \tilde{\Delta}_M\right)^{-1}\left(\widetilde{N} + \tilde{\Delta}_N\right) \tag{7}$$

where $\tilde{\Delta}_M$ and $\tilde{\Delta}_N$ are the unknown uncertainties. Also, $\tilde{\Delta}_M$ and $\tilde{\Delta}_N$ are stable transfer functions, such that

$$\|[\tilde{\Delta}_M \quad \tilde{\Delta}_N]\|_\infty < \epsilon \tag{8}$$

where ϵ is the stability margin of the robust H-infinity controller (Glad and Ljung, 2000). In addition, Fig. 6 shows the left coprime factor perturbed system.

Next, the robust H-infinity controller with guaranteed closed-loop stability and robust stability is obtained by applying the loop shaping method, which includes the design of pre-compensator weights W_1 and post-compensator weights W_2. In general, W_1 is designed as a PID controller, while W_2 is designed as a low-pass filter to achieve the expected control performance, such as high gain in low frequencies, low gain in high frequencies, and the desired stability margin (Sebastian and Salapaka, 2005), (McFarlane and Glover, 1992). The design procedure of the robust H-infinity control with loop shaping consists of two steps. First, the shaped model G_s shown in Fig. 7(a) is defined as the multiplication of the loop shaping weights with the nominal model G, such that

$$G_s = W_2 G W_1 \tag{9}$$

where G is the MIMO position transfer function matrix in (1). To simplify the design of the loop shaping compensators, both W_1 and W_2 are considered as a diagonal matrix, while the non-diagonal terms are set to zero. To be more specific, the transfer function of W_1 is designed as

$$W_1 = 1 + 3000 \cdot \frac{1}{s} + 10^{-6} \cdot s \tag{10}$$

and the transfer function of W_2 is designed as

$$W_2 = \frac{500}{s+500} \tag{11}$$

Second, the robust H-infinity controller K_∞ with associated robustness property is synthesised to stabilise the shaped model G_s in (9) and to maximise the stability margin based on the robust H-infinity control theory (Sebastian and Salapaka, 2005). Therefore, the final feedback controller K shown in Fig. 7(b) is given by

$$K = W_1 K_\infty W_2 \tag{12}$$

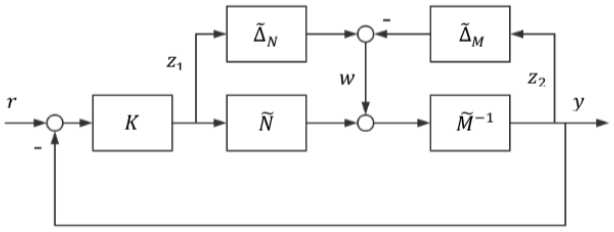

Fig. 6. Left Coprime Factor Perturbed System.

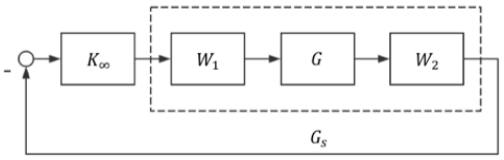

(a)

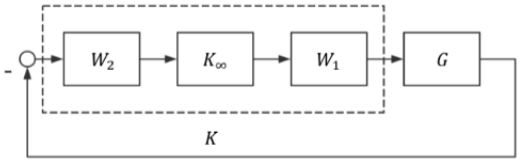

(b)

Fig. 7. The Loop Shaping Design Procedure.

The H-infinity optimisation problem is solved by the MATLAB *ncfsyn* command. In addition, the singular values of the nominal model G and the shaped model G_s, with the designed loop shaping weights, are presented in Fig. 8. This shows that the first resonant peak of the shaped model G_s is lower than the steady-state value of the nominal model G.

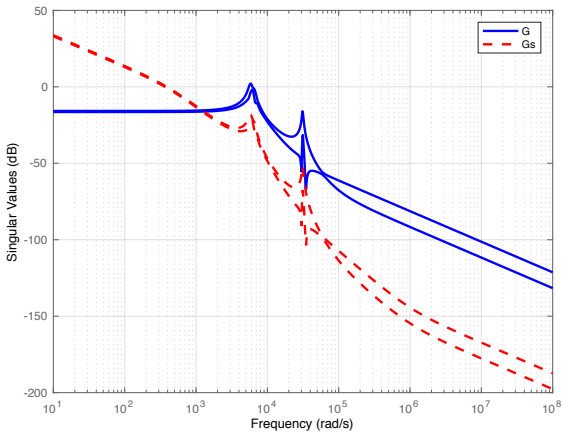

Fig. 8. The Singular Values of Nominal Model G and Shaped Model G_s.

4. CASE STUDY

In this section, two designed controllers are implemented to the $NPS-\theta\gamma-2M$ tip tilt nanopositioning stage and their control performance are discussed and compared based on the system step response and PRBS frequency response. The simulation result is obtained from the MIMO position model in MATLAB/Simulink, while the experimental result is obtained from a $NPS-\theta\gamma-2M$ tip tilt nanopositioning stage in the lab. In particular, the control performance is analysed according to the system settling time and overshoot in the time domain, and the closed-loop bandwidth in the frequency domain. The system response is assumed to reach the steady-state when the system output error is bounded within 0.1% of the final value, which is almost equal to a unit nanoscale error.

4.1 Benchmark SISO Integral Control

The SISO integral control is implemented using Fleming's method (Fleming and Leang, 2014). The control performance of the experimental result is presented in Table 3; this shows that the system response of channel x has a smaller overshoot and is faster than channel y. Moreover, the closed-loop bandwidths of channels x and y are 2.5% and 2.1% of the first resonant frequency respectively, which accords with Fleming's results that the maximum bandwidth of simple PI

feedback control is limited to 2% of the first resonant frequency (Fleming and Leang, 2014).

Channel	Settling time (sec)	Overshoot (%)	Bandwidth (rad/sec)
X	0.0876	0.4	156
Y	0.1597	1.1	122

Table 3. The Control Performance of SISO Integral Control.

Fig. 9 shows the simulated and experimental step responses for diagonal channel xx and cross-coupling channel xy. Here, the input channel x is given the step signal, while the input channel y is set to zero. The output error reduces to approximately zero in the steady-state, which satisfies the control specification of the SISO integral control. The cross-coupling effect on channel xy has a slight variation, which is around the scale of 10^{-2} V when the input channel x has a unit step changed. In addition, Fig. 10 shows the closed-loop frequency response of diagonal channel xx and cross-coupling channel xy.

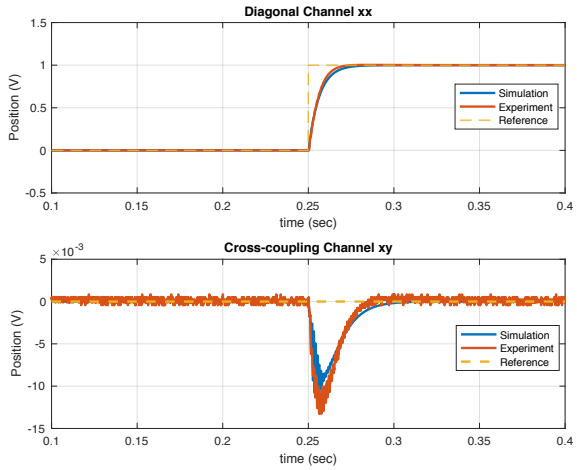

Fig. 9. Step Response of SISO Integral Control.

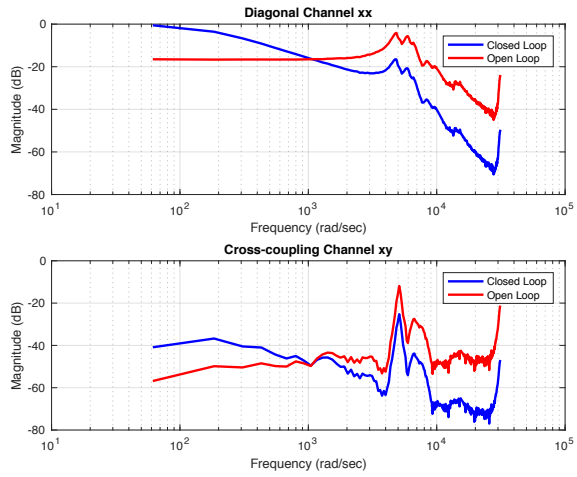

Fig. 10. Frequency Response of SISO Integral Control.

4.2 MIMO Robust H-infinity Control with Loop Shaping Design

The MIMO robust H-infinity control with loop shaping design follows the Glover-McFarlane method (McFarlane and Glover, 1992). Table 4 presents the control performance of the experimental result. It shows that the nanopositioning stage controlled by the designed robust H-infinity controller has a faster response and a higher closed-loop bandwidth compared with the SISO integral control. To be more specific, the closed-loop bandwidths of channel x and y are 460 and 530 rad/sec, respectively, which is three to four times higher than the SISO integral control. Thus, the result meets the design objectives of reducing the system response time and improving the closed-loop bandwidth. Nonetheless, the main drawback is the overshoot in the transient response, which is more significant than that in the SISO integral control.

Channel	Settling time (sec)	Overshoot (%)	Bandwidth (rad/sec)
X	0.0416	10	460
Y	0.0331	9	530

Table 4. The Control Performance of MIMO Robust H-infinity Control with Loop Shaping Design.

Fig. 11 shows the result of the simulated and experimental step responses. It is noted that the output signal tracks the reference signal with the same magnitude but in the opposite direction, as the robust H-infinity controller is implemented in the positive feedback structure. Furthermore, the experimental response has a more significant overshoot and a slightly longer settling time than the simulated response. The reason for the discrepancy between the simulation and experimental result may be the modelling mismatching and the neglected system nonlinearity problems. Also, the micro oscillation in the experimental response is affected by the noise and disturbance from the system itself and the environment. Besides, Fig. 11 reveals the system cross-coupling effect and shows that the variation of the cross-coupling channel xy is around the scale of 10^{-3} V when input channel x has a step change. The magnitude of the cross-coupling effect is ten times smaller than the SISO integral control, as the whole multivariable position models were considered in the MIMO robust H-infinity control design scheme. In addition, Fig. 12 shows the closed-loop frequency response of both diagonal channel xx and cross-coupling channel xy.

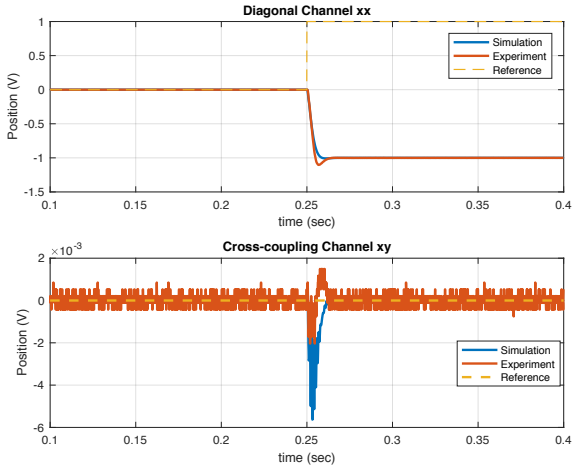

Fig. 11. Step Response of MIMO Robust H-infinity Control with Loop Shaping Design. It is noted that the scale of y-axis is different from Fig. 9.

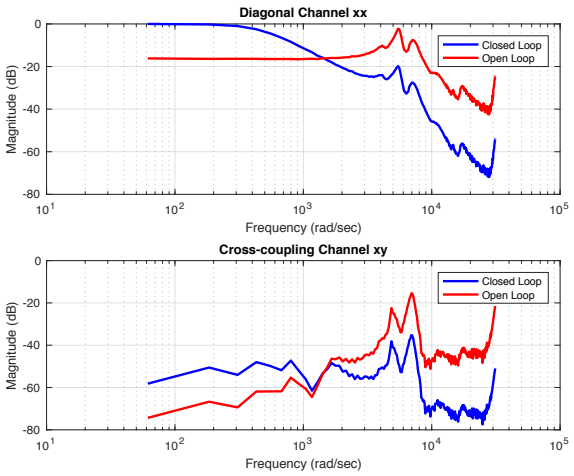

Fig. 12. Frequency Response of MIMO Robust H-infinity Control with Loop Shaping Design.

From the above system step and frequency responses, it is clear that the $NPS-\theta\gamma-2M$ tip tilt nanopositioning stage controlled by the MIMO robust H-infinity control with loop shaping design has a faster tracking response, a higher closed-loop bandwidth and lower cross-coupling effect compared with the SISO integral control. Therefore, the design of the MIMO robust H-infinity control achieves the main objective. Moreover, the resulting system can track a faster reference signal and can be used in faster nanopositioning applications.

5. CONCLUSIONS

In the paper, we have studied the tip tilt nanopositioning stage and carried out the modelling and control design for the $NPS-\theta\gamma-2M$ tip tilt nanopositioning stage to achieve the desired tip tilt nanopositioning control. Accordingly, the conclusion can be divided into two parts: one concerned with the modelling, and the other with the control design.

In terms of modelling, the discrete OE model structure with different orders and the data-driven system identification approach has been applied to establish the MIMO linear position model for the $NPS-\theta\gamma-2M$ tip tilt nanopositioning stage. Moreover, the analysis of nonlinear distortion level for position model following Godfrey's method proves that the linear dynamics dominate most of the system dynamics below the first resonant frequency. It is, therefore, a reasonable assumption to use the linear model to approximate the practical nonlinear system. Additionally, the modelling validation by the non-parametric method shows that the best fit linear OE model from the MATLAB System Identification Toolbox captures most of the system dynamics in the operating range.

In addition, a MIMO H-infinity control design method was developed and implemented for the $NPS-\theta\gamma-2M$ tip tilt nanopositioning stage. This was also compared with a benchmark integral only control design. Both controllers were tested in both the simulation and the experiment. The benchmark SISO integral control following Fleming's design method has a relatively slower response, and the closed-loop bandwidth is around 2% of the first resonant frequency, as expected. By contrast the MIMO robust H-infinity control with loop shaping design has a faster response that is two to five times faster than the SISO integral control, and also a higher closed-loop bandwidth, which is 7% to 9% of the first resonant frequency. Moreover, the cross-coupling effect was reduced to ten times smaller than the SISO integral control, as the whole multivariable models were considered in the design scheme of the MIMO robust H-infinity control.

Future research is feasible for studying the physical properties of the tip tilt nanopositioning stage and its nonlinearity. The MIMO force model can be introduced and built by system identification and the experiment can be strengthened by testing different reference trajectory such as sinusoidal or triangular signals. Furthermore, the other advanced control theories could be applied to improve control performance.

REFERENCES

Bongers, P. M. M. and Bosgra, O. H. (1993). Normalized Coprime Factorizations for Systems in Generalized State-Space Form. *IEEE Transactions on Automatic Control*, 38(2), pp. 348–350.

Das, S. K., Pota, H. R. and Petersen, I. R. (2015). A MIMO double resonant controller design for nanopositioners. *IEEE Transactions on Nanotechnology*. IEEE, 14(2), pp. 224–237.

Devasia, S., Eleftheriou, E. and Moheimani, S. O. R. (2007). A Survey of Control Issues in Nanopositioning. *IEEE Transactions on Control Systems Technology*, 15(5), pp. 802–823.

Eielsen, A. A., Vagia, M., Gravdahl, J. T. and Pettersen, K. Y. (2014). Damping and tracking control schemes for nanopositioning. *IEEE/ASME Transactions on Mechatronics*. IEEE, 19(2), pp. 432–444.

Fleming, A. J. and Leang, K. K. (2014). *Design, Modeling and Control of Nanopositioning Systems*. Advanced in Industrial Control. Springer International Publishing, Switzerland, 3rd edition.

Glad, T. and Ljung, L. (2000). *Control Theory: Multivariable and Nonlinear Methods*. London: Taylor&Francis.

Godfrey, K. R., Tan, A. H., Barker, H. A. and Chong, B. (2005). A survey of readily accessible perturbation signals for system identification in the frequency domain. *Control Engineering Practice*.

Gu, G. Y., Zhu, L. M., Su, C. Y., Ding, H. and Fatikow, S. (2016). Modeling and control of piezo-actuated nanopositioning stages: A survey. *IEEE Transactions on Automation Science and Engineering*, 13(1), pp. 313–332.

Kara-Mohamed, M. and Heath, W. P. (2016). Classical Tuning of Force Feedback Control for Nanopositioning Systems with Load Variations. *IFAC-PapersOnLine*. Elsevier B.V., 49(21), pp. 649–655.

Kara-Mohamed, M., Heath, W. P. and Lanzon, A. (2015). Enhanced Tracking for Nanopositioning Systems Using Feedforward/Feedback Multivariable Control Design. *IEEE Transactions on Control Systems Technology*, 23(3), pp. 1003–1013.

Ljung, L. (1999). *System identification: theory for the user*. 2nd edition. Upper Saddle River, New Jersey: Prentice Hall.

McFarlane, D. and Glover, K. (1992). A loop-shaping design procedure using H_sub infinity Synthesis. *IEEE Transactions on Automatic Control*, 37(6), pp. 759–769.

Schoukens, J., Pintelon, R., Dobrowiecki, T. and Rolain, Y. (2003). Identification of Linear Systems with Nonlinear

Distortions. *IFAC Proceedings Volumes (IFAC-PapersOnline)*, 36(16), pp. 1723–1734.

Sebastian, A. and Salapaka, S. M. (2005). Design methodologies for robust nano-positioning. *IEEE Transactions on Control Systems Technology*, 13(6), pp. 868–876.

Skogestad, S. and Postlethwaite, I. (2005). *Multivariable Feedback Control: Analysis and Design.* 2nd edition. Chichester: John Wiley.

Vaqueiro-Contreras, M. (2015). *System Identification for Nano-Scale Control*. M.Phil. thesis, The University of Manchester.

Yong, Y. K., Aphale, S. S. and Reza Moheimani, S. O. (2008). Design, analysis and control of a fast nanopositioning stage. *IEEE/ASME International Conference on Advanced Intelligent Mechatronics*, AIM, (August), pp. 451–456.

Appendix A. Frequency Response of MIMO Position Model

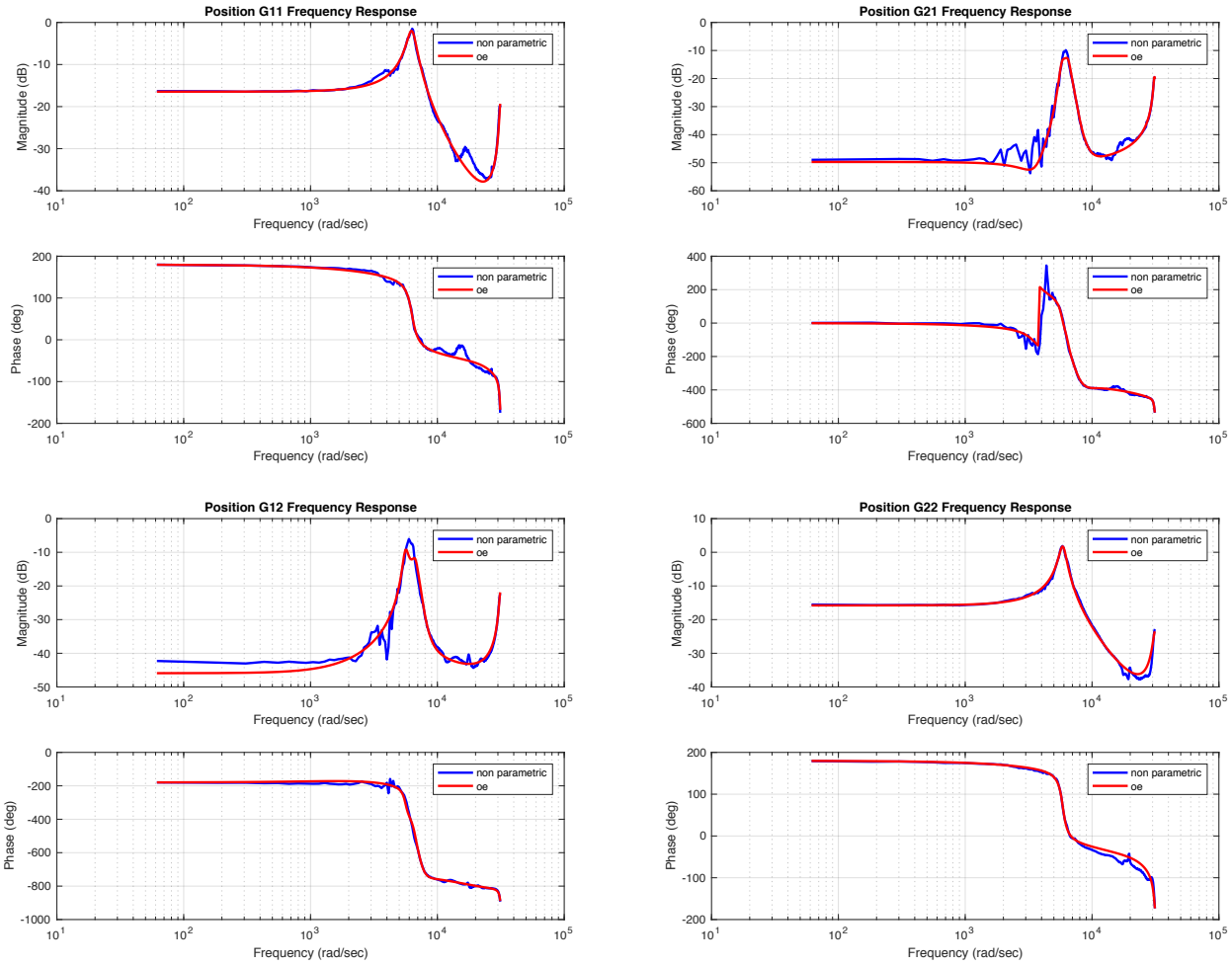

Appendix B. Discrete Transfer Function of MIMO Position Model

$$G_{11} = \frac{-0.01615z^{-1} - 0.04643z^{-2}}{1 - 1.007z^{-1} - 0.3023z^{-2} + 1.078z^{-3} - 0.3527z^{-4}}$$

$$G_{12} = \frac{0.00616z^{-1} - 0.03272z^{-2} + 0.07203z^{-3} - 0.08673z^{-4} + 0.05777z^{-5} - 0.01751z^{-6} - 0.001315z^{-7} + 0.001884z^{-8}}{1 - 3.889z^{-1} + 6.368z^{-2} - 4.251z^{-3} - 1.469z^{-4} + 5.052z^{-5} - 4.012z^{-6} + 1.481z^{-7} - 0.1948z^{-8}}$$

$$G_{21} = \frac{0.006383z^{-1} - 0.02373z^{-2} + 0.03607z^{-3} - 0.01939z^{-4} - 0.01492z^{-5} + 0.03098z^{-6} - 0.02048z^{-7} + 0.005818z^{-8}}{1 - 2.624z^{-1} + 1.809z^{-2} + 2.466z^{-3} - 4.836z^{-4} + 2.156z^{-5} + 1.536z^{-6} - 1.655z^{-7} + 0.6719z^{-8}}$$

$$G_{22} = \frac{-0.01922z^{-1} - 0.05236z^{-2}}{1 - 0.9942z^{-1} - 0.3008z^{-2} + 0.968z^{-3} - 0.2326z^{-4}}$$